Stereoelectronic factors in CO, NO and O 2 binding to heme from vibrational spectroscopy and DFT analysis

ARTICLE *in* COORDINATION CHEMISTRY REVIEWS · SEPTEMBER 2001

Impact Factor: 12.24 · DOI: 10.1016/S0010-8545(01)00384-8

ELSEVIER

Coordination Chemistry Reviews
219–221 (2001) 923–936

COORDINATION CHEMISTRY REVIEWS

www.elsevier.com/locate/ccr

Stereoelectronic factors in CO, NO and O_2 binding to heme from vibrational spectroscopy and DFT analysis

Thomas G. Spiro [a,*], Marek Z. Zgierski [b], Pawel M. Kozlowski [a,1]

[a] *Frick Laboratory, Department of Chemistry, Princeton University, Princeton, NJ 08544, USA*
[b] *Steacie Institute for Molecular Science, National Research Council of Canada, Ottawa, Canada, K1A OR6*

Received 13 October 2000; accepted 26 March 2001

Contents

Abstract

CO, NO and O_2 are physiologically important molecules whose biochemistry is largely mediated by transient binding to transition metal ions, especially to Fe(II) in the heme

* Corresponding author. Tel.: +1-609-258-3907; fax: +1-609-258-0348.
E-mail address: spiro@princeton.edu (T.G. Spiro).
[1] Present address: Department of Chemistry, University of Louisville, Louisville, KY 40292, USA.

PII: S0010-8545(01)00384-8

prosthetic group. The mechanism of action is determined by interactions of the FeXO unit (X = C, N or O) with protein residues in the heme pocket. These interactions can be assessed via the FeXO vibrational frequencies, which are available from infrared (IR) and resonance Raman (RR) spectra. The vibrational frequencies are largely determined by the donor properties of the proximal ligand, and by the electrostatic field of the residues on the distal side of the bound XO. This field polarizes the FeXO unit and modulates backbonding from Fe to XO, resulting in anticorrelated shifts in the XO and FeX stretching frequencies. Empirically derived trends in the vibrational frequencies are supported by ab initio calculations using the density functional theory (DFT). DFT analysis also provides the correct geometries of the unconstrained FeXO units, and has been used to investigate the energy required for distortion from the equilibrium geometry. This energy is modest, even for the linear FeCO unit, indicating that steric forces from distal protein residues are not major determinants of the ligand binding energy. DFT analysis has also illuminated the contentious issue of the extent of FeCO distortion in myoglobin. While X-ray crystallographic analyses have yielded a range of geometries, the vibrational data are all consistent with an undistorted upright structure. However, DFT analysis of the sensitivity of IR polarization measurements, and of the νCO/νFeC backbonding correlation, indicates that the data allow up to 0.5 Å off-axis displacement of the O atom in the FeCO unit. The energy cost of this much displacement is small, ca. 0.8 kcal mol^{-1}, a value that is consistent with binding energy measurements on myoglobin mutants.

1. Introduction

A major theme in coordination chemistry is the ability of low-valent transition metal ions to bind the diatomic molecules CO, NO and O_2, because the unoccupied XO π^* orbitals are well matched, spatially and energetically, to occupied metal d_π orbitals. The binding results from a synergic flow of electrons from metal to ligand in the π system (backbonding) and from ligand to metal in the σ system. Nature has adapted these interactions to utilize CO, NO and O_2, either as reactants or as biochemical signals. All three molecules bind to the Fe(II) ion of the heme prosthetic group in heme proteins. These are diverse macromolecules, which have evolved to carry out a variety of physiological functions in response to the binding event. Since the chemical structure of the heme–XO adduct is the same for all heme proteins, the events subsequent to binding must reflect differences in the interactions of the FeXO unit with the surrounding protein. Elucidating these interactions has been a major theme in biostructural research, and has been pursued with the full arsenal of biophysical techniques. Within this arsenal, vibrational spectroscopy plays a prominent role because the vibrational frequencies are sensitive to molecular conformation, and to chemical interactions. These frequencies are available from infrared (IR) and Raman spectroscopy, which can also yield useful information from band intensities and polarizations. An important development in the application of vibrational spectroscopy has been the increasing power of ab initio calculations, particularly with the advent of the density functional theory (DFT), to calculate the geometries as well as the vibrational spectra of complex molecules,

including metalloporphyrins and their adducts [1]. This review summarizes the current status of efforts to bring vibrational spectroscopy and DFT analysis to bear on the nature of FeXO interactions in heme proteins.

2. CO adducts

2.1. Backbonding and the electronic environment

The Fe–C stretching vibration, νFeC, is readily detected as a band of moderate intensity near 500 cm^{-1} in resonance Raman (RR) spectra of heme–CO adducts [2]. The band is enhanced in resonance with the porphyrin π–π^* transitions because the Fe d_π orbitals overlap with π^* orbitals from the porphyrin ring as well as from the bound CO, so that the π–π^* potential is displaced along the Fe–C stretching coordinate. The displacement along the C–O stretching coordinate is smaller, so that νCO is seen only weakly in RR spectra, but it is strong in IR spectra, because stretching the C–O bond generates a large dipole, thanks to the π overlap. The IR band is readily detected even in heme proteins, because the νCO frequency, ca. 1950 cm^{-1}, is in a region without interfering protein bands. The FeCO bending vibration can often be found in RR spectra as a weak band near 570 cm^{-1}, and is identified via a characteristic isotope shift pattern [2]. The frequency is much more sensitive to ^{18}O than to ^{13}C substitution because the O atom motion is much greater than the C atom motion in the bending vibration. The bending mode lacks an RR enhancement mechanism unless the heme–CO symmetry is lowered from C_{4v}, and it is not observed in protein-free heme–CO adducts (provided there is no encumbering superstructure). The required symmetry lowering may reflect an actual distortion of the heme–CO geometry, or merely asymmetry in the electrostatic potential of the surrounding protein [3].

The νFeC and νCO frequencies in different proteins are quite variable, but the two frequencies are consistently found to be negatively correlated: as one increases, the other decreases (Fig. 1). This is the expected effect of variations in backbonding. Because the d_π electrons are transferred to the CO π^* orbitals, the CO bond order diminishes while the FeC bond order is augmented when backbonding is increased. The extent of backbonding is influenced by polarization of the bound CO by residues in the heme pocket. For example, a positively charged arginine distal to the CO in horseradish peroxidase produces a high νFeC and low νCO [4], while for a myoglobin mutant in which the CO faces the lone pair of a serine hydroxyl group, νFeC is low while νCO is high [5]. Native myoglobin is found in the middle of the backbonding correlation, but when the distal histidine is replaced by another residue having a non-polar sidechain, the νFeC/νCO data pair move down the correlation [3], showing that the distal histidine provides positive polarization, consistent with a weak H-bond from a proton on the histidine N_ε atom [6]. The effect of distal charges has been modeled theoretically [7], and variations of νCO in a series of structurally characterized Mb mutants have been satisfactorily computed via the electrostatic field in the heme pocket [8].

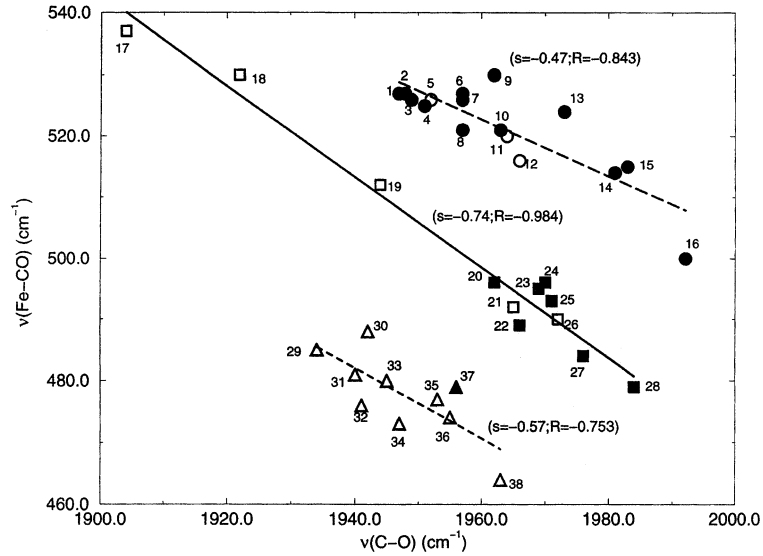

Fig. 1. Plot of observed ν(Fe–CO) vs. ν(C–O) frequencies in Fe(II)CO heme proteins and model complexes. (From Ref. [11], where the numbering key may be found.) The top dashed line is for five-coordinate CO adducts (circles); the bottom two lines are for complexes in which the FeCO is ligated by a histidine (squares) or by a thiolate or histidinate ligand (triangles). The open symbols represent protein data; closed symbols are porphyrin model compounds. The slopes and correlation coefficients are given in parentheses.

Protein-free CO adducts of Fe(II) porphyrins follow the same backbonding correlation as the proteins, and can be moved up and down along the correlation by changing the solvent, or by having a superstructure with positive or negative dipoles near the CO [3]. Backbonding can also be altered by substituents on the porphyrin. Thus, phenyl substituents at the C_m positions are less electron-donating than ethyl groups at the C_β positions, so that tetraphenylporphine is lower on the correlation than is octaethylporphyrin.

2.2. Axial ligands

The correlation described in the preceding section holds for proteins and models in which the axial coordination site *trans* to the CO is occupied by a neutral imidazole ligand. However, if the imidazole is deprotonated, or if the axial ligand is a thiolate, as in cytochrome P450, then νFeC is strongly depressed (Fig. 1). The νFeC/νCO points now fall on a new line, parallel to the imidazole line, but shifted to lower νFeC [9]. This shift reflects the competition for the Fe d_{z^2} orbital between the σ lone pairs on CO and on the axial ligand. Thiolate and imidazolate are stronger donors than neutral imidazole; even though they also enhance backbonding to the CO, the effect of the σ competition is to weaken the Fe–C bond. Model compound data indicate that thioether adducts fall on the same correlation as the

neutral imidazole complexes [10], so that the charge on the axial ligand seems to be the main determinant of the *trans* ligand effect. Intermediate cases found in proteins (e.g. some forms of the peroxidases), in which the νFeC/νCO data pairs fall between the anion and neutral ligand lines, may reflect partial neutralization of anions via H-bonding.

A correlation having higher νFeC values is expected when the *trans* axial coordination site is left vacant, since there is no σ competition. This is indeed observed, but the five-coordinate line is found to have a smaller slope than the six-coordinate lines [11] (Fig. 1). The slope of the correlation is the sensitivity of νFeC to backbonding, and the higher sensitivity of six-coordinate heme–CO adducts reflects the Fe–C bond lengthening produced by the σ competition. The longer bond produces a greater change in the d_π–π^* overlap per unit of backbonding. The C–O bonds are not directly affected by the σ competition, and therefore the slope of the correlation is increased. These effects have been reproduced with DFT calculations on model heme–CO adducts [11–13]. The model has the full porphine ring, and an imidazole axial ligand, *trans* to the CO. An accurate geometry is obtained, and Fe–C bond lengthening upon axial ligation is correctly predicted [12]. The vibrational frequencies are close to those observed (Table 2).

When electron-withdrawing (F) or -donating (NH_2) substituents are added to the ring, νFeC and νCO correlate negatively, as expected [11]. Moreover, when the imidazole ligand is removed, or replaced by methyl thiolate, the lines shift to higher and lower νFeC values, respectively. The calculated slopes are twice the experimental ones, indicating that DFT overestimates the rate of change of the d_π–π^* overlap, but the ratios of the slopes are in excellent agreement with experiment. Thus, DFT captures the essential features of backbonding and axial ligand effects.

2.3. Deformability; steric effects

The issue of FeCO distortion from linearity has been a vexing one for many years. The first high-resolution X-ray structure determination of the myoglobin–CO adduct gave FeCO angles of 120–140°, although the CO was disordered and the electron density was fitted to two conformers, each with Fe–C bonds normal to the heme [14]. Neutron diffraction gave similar results [15]. However, subsequent X-ray structures gave smaller degrees of distortion [16–18], and it now seems likely that the earlier structures suffered from partial oxidation to met-myoglobin, in which a water molecule is bound to the heme Fe(III). Still, the newer structures give a range of modest distortions from a strictly upright FeCO geometry (Fig. 2).

There had long been skepticism of the possibility of significant FeCO distortion on energetic grounds, since distortion is at the expense of π bonding. The FeCO bending frequency, 570 cm^{-1}, is high, suggesting a stiff FeCO unit. Indeed, it is higher than the Fe–C stretching frequency. This unusual circumstance has led to suggestions that the 570 cm^{-1} RR band be reassigned to an overtone [19] or combination [20] band, but the issue has been resolved in favor of the original assignment [21,22]. If simple harmonic motion were assumed, then the energy required to produce significant FeCO bending would reach tens of kcal mol^{-1} [9].

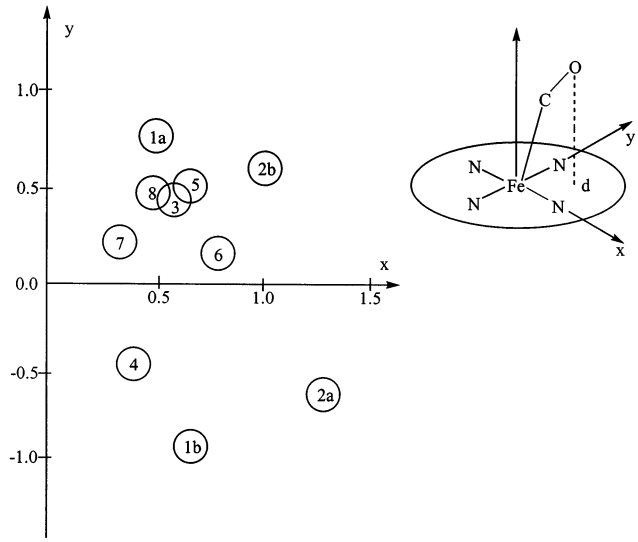

Fig. 2. Projection of the O atom displacement from the heme z-axis in MbCO crystal structures; points 1a and 1b, native $P2_1$ MbCO crystal, PDB file 1mbc, Ref. [14]; points 2a and 2b, native $P2_1$ MbCO crystal, PDB file 2mb5, Ref. [15]; point 3, 'wild-type' D122N mutant of sperm whale myoglobin that crystallizes in a $P6$ space group, PDB file 2mgk, Ref. [16a]; points 4, 5, 6, native $P2_1$ MbCO crystals at pH4, 5 and 6, PDB files 1spe, 1vxc, 1vxf, Ref. [16b]; point 7, $P2_1$ MbCO crystal (1.15 Å resolution) PDB file1bzr, Ref. [17]; point 8, $P2_1$ MbCO crystal (1.2 Å resolution) PDB file1a6g, Ref. [18] (from Ref. [32]).

However, DFT analysis revealed that the high bending frequency results from a large interaction force constant between the bending and tilting coordinates of the FeCO unit [23,24]. This interaction arises because both coordinates diminish π bonding, either with the CO or with the porphyrin ligand. As the entire FeCO unit is tilted, within the porphyrin frame, bending is facilitated. The result is considerable mixing between the bending and tilting coordinates, with a large separation between the two frequencies. The interaction also lowers the energy required for FeCO distortion dramatically. A minimum energy distortion path was calculated by constraining the O atom to fixed displacements from the heme normal through the Fe atom, and allowing the entire structure to relax under this constraint (Fig. 3) [13,24]. The energy required for a 0.6 Å displacement, a value within the range of the X-ray structures, is only ca. 0.8 kcal mol^{-1}. Density-functional molecular dynamics simulations of a heme–CO adduct show rapid excursions of the O atom by up to 0.6 Å [25].

Seemingly direct evidence against FeCO distortion has come from measurements of the polarization of the CO stretching IR band on oriented single crystals [26] and on molecules in solution which are photoselected with an ultrafast laser pulse [27]. Both types of measurements have given angles for the IR transition dipole within 7° of the heme normal. However, the dipole angle is not the same as the bond angle, because stretching of the CO bond displaces electrons throughout the molecule, thanks to the extensive π bonding. DFT-computed dipoles along the

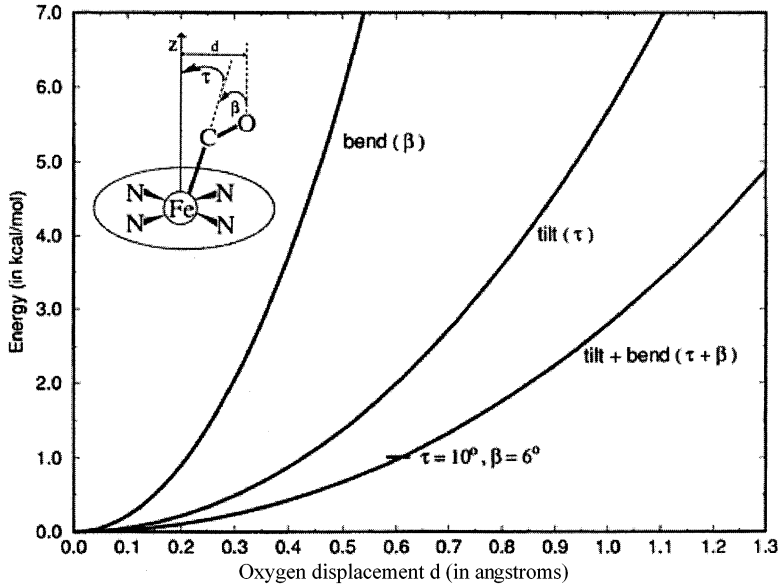

Fig. 3. Harmonic energies calculated via DFT for bending alone (β), tilting alone (τ), and a minimum energy combination of bending and tilting (from Ref. [24b]).

minimum energy distortion path indicate that the dipole vector lags significantly behind the CO bond vector (Fig. 4), and that a 7° dipole angle implies a 0.6 Å O atom displacement from the heme normal [24b]. Another test of distortion is provided by the backbonding correlation of νFeC and νCO (Fig. 1). Since FeCO distortion diminishes π bonding, deviations from the backbonding correlation are expected. However, there is some scatter to the data, and DFT calculations suggest that O atom displacements up to 0.5 Å might be accommodated by the scatter [13]. Thus, the vibrational data give no evidence in favor of FeCO distortion, but can accommodate an O atom displacement up to 0.5 Å. It should be noted that ^{13}C- and ^{18}O-NMR data have been extensively analyzed by Oldfield and co-workers [28], and found to be consistent with an undistorted FeCO unit in MbCO. However, the tolerance of the data to small distortions has not been quantitatively addressed.

2.4. Mechanism of CO/O_2 discrimination

The finding of FeCO distortion in MbCO gave rise to the idea that steric hindrance by a distal histidine residue is the mechanism for discriminating against CO binding [29]; the distal imidazole ring is displaced from its position above the Fe atom in deoxyMb. FeO_2, being naturally bent, would be less subject to steric hindrance. The binding energy difference between CO and O_2 is reduced by ca. 4 kcal mol^{-1} in Mb relative to protein-free heme.

However, the evidence from site-directed mutagenesis in Mb [30] weighs strongly in favor of H-bonding from the distal imidazole as the main factor in establishing

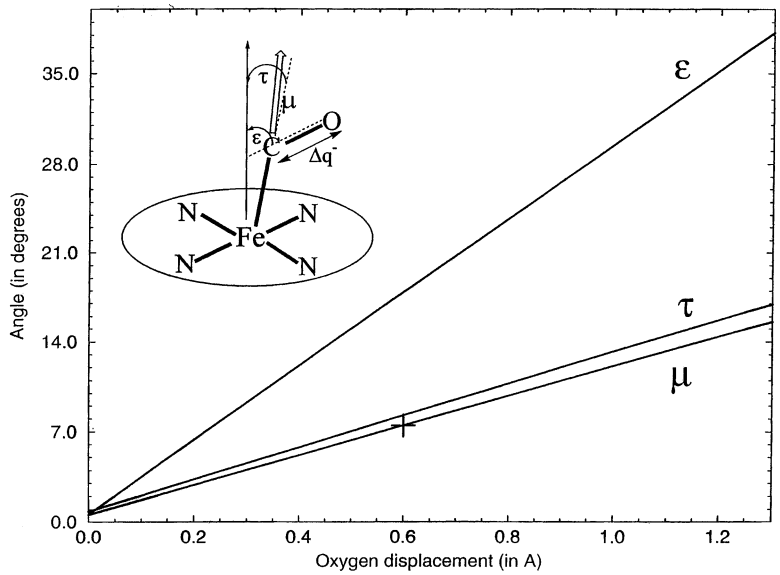

Fig. 4. Calculated transition dipole direction along the minimum energy distortion path, compared with the CO bond vector and FeC tilt angle. Single crystal polarized IR on MbCO gives $6.9 \pm x°$, while ps IR photoselection in solution gives $< 7°$, corresponding to < 0.6 Å O atom displacement (+) (from Ref. [24b]).

the discrimination against CO and in favor of O_2. A weak H-bond is already present for FeCO, as indicated by the backbonding correlation (see above) and by the observation of D_2O sensitivity of the vibrational bands [6], and the H-bond becomes much stronger for FeO_2 [31] because more electron density is transferred from the heme to the ligand for O_2 than for CO. Analysis of the ligation rate and equilibrium constants for mutants having hydrophobic residues in place of the distal histidine [30] has provided an estimate of only 0.6 kcal mol^{-1} for the steric energy inhibiting CO binding [32], in gratifying accord with the magnitude of the DFT-computed distortion energy.

3. NO and O_2 adducts

Vibrational data are sparser for NO and O_2 adducts than for CO adducts of heme. RR enhancements of the FeXO vibrations are weaker for FeNO and FeO_2, probably because backbonding to the XO ligand is stronger and the d_π electrons are less equally shared between the XO and the porphyrin π^* orbitals. The depletion of backdonation to the porphyrin orbitals can be seen in upshifts of porphyrin skeletal modes, which are greater for NO and O_2 than for CO [33]. In addition, the νXO frequencies are in the range of porphyrin skeletal modes, which produce much stronger RR bands. IR spectra additionally suffer interference from protein bands.

Nevertheless, a number of careful experimental studies, often utilizing isotope difference spectra, have provided a useful database (see Ref. [12] for a summary).

3.1. Geometry; valence isomers

Binding to heme differs in important respects for NO and O_2, relative to CO. The increase in nuclear charge from C to N to O lowers the π^* energies of the XO molecules in the same order, leading to increased charge transfer from Fe to XO. This is seen clearly in the XO stretching frequencies, which are decreased upon binding, relative to the free molecule, to a greater extent for NO (ca. 1600 vs. 1877 cm^{-1}) than for CO (ca. 1950 vs. 2145 cm^{-1}), and to a still greater extent for O_2 (ca. 1150 vs. 1555 cm^{-1}). For FeO_2, the frequency is as low as in the superoxide ion, indicating transfer of essentially a full electronic charge.

In addition, FeCO is linear while FeNO and FeO_2 are bent, because the extra electrons, one for NO and two for O_2, are antibonding with respect to a linear geometry. The consequences can be viewed in the light of the valence isomer model [12] illustrated in Fig. 5. (The classic paper of Hoffman et al. [34] can be consulted for a more detailed account of the molecular orbital interactions.) In this model, isomer I is linear, while isomer II is bent, and one of the XO π bonds is replaced by a non-bonding lone pair-type orbital, which is directed away from the Fe, along the bisector of the FeCO angle. This orbital is empty in FeCO, so isomer II is unpopulated, but it accommodates the two extra electrons of O_2, leading to full population of isomer II, as indicated by ca. 120° bond angle for FeO_2 (Table 1).

Both isomers are populated for FeNO, which has one extra electron. (We note that the two populations cannot be distinguished spectroscopically because the nuclear positions are averaged on the vibrational time scale.) The bond angle is ca. 140°, indicating a dominant isomer II population, but the influence of isomer I can

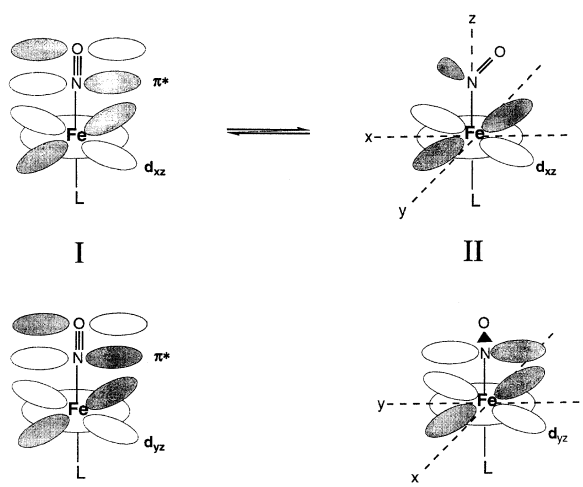

Fig. 5. Valence isomer bonding of model for XO adducts of Fe(II) porphyrins (from Ref. [12]).

Table 1
Heme Fe(II)XO structural parameters (from Ref. [12])

Compound	Fe–XO (Å)	X–O (Å)	Fe–X–O (°)	Fe–N_P (Å)	δ_{oop} [a] (Å)	Fe–L (Å)
Five-coordinate CO						
Deut(THF)(CO)	1.706(5)	1.144(5)	177.4(9)	1.980	–	2.127(4)
DFT [b]: Fe(P)	1.727	1.171	180.0	2.013	0.186	–
Six-coordinate CO						
TPP(py)(CO)	1.77(2)	1.12(2)	179(2)	2.015	-	2.10(1)
DFT [b]: Fe(P)(py)	1.781	1.168	180.0	2.028	0.186	2.102
Five-coordinate NO						
OEP(NO)	1.722(2)	1.167(3)	144.4(2),	1.991(3) 2.016(1)	0.29	–
OEP(NO)	1.7307(7)	1.168(11)	142.74(8)	1.999(1) 2.020(4)	0.27	–
TPP(NO)	1.717(7)	1.122(12)	149.2(6)	2.001(3)	0.211(5)	–
2,6-Dichloro-TPP(NO)	1.703(8)	–	138.8(9)	2.004	0.31	–
Octabromo-TPP(NO)	1.75(6)	1.418(73)	146.4(2)	1.986	0.37	–
Average	1.723	1.219	145.1	2.002	0.28	–
DFT [b]: Fe(P)	1.716	1.198	142.0	2.020	0.15	–
Six-coordinate NO						
TPP(1-MeIm)(NO)	1.743(4)	1.14 1.12	142.1(6), 138.3(11)	2.008(9,4)	0.05	2.180(4)
TPP(4-MePip)(NO) · $CHCl_3$	1.721	1.14	138.5(11)	2.328 (10)	0.09	2.328(10)
TPP(4-MePip)(NO)	1.740(7)	1.11	143.7(6)	2.463(7)	0.11	2.463(7)
Average	1.735	1.13	140.7	2.266	0.08	2.324
DFT [b]: Fe(P)(py)	1.786	1.201	141.6	2.03	0.04	2.066
Five-coordinate O_2						
DFT [b]: Fe(P)	1.715	1.314	122.386	2.01	0.22	–
Six-coordinate O_2						
TPivP(2-MeIm)	1.898(7)	1.22(2)	129	1.95(6)	−0.086	2.107(4)
TPivP(1-MeIm)	1.75(2)	1.16(8)	131	1.996(4)	0.03	2.07(2)
TPivP(1,2-Me_2Im)	1.77(3)	–	–	1.99(3)	–	2.29(4)
Average	1.806	1.19	130	1.979	−0.028	2.156
DFT [b]: Fe(P)(py)	1.776	1.311	122.9	2.023	−0.019	2.024

P, porphine; py, pyridine; TPP, tetraphenylporphyrin; OEP, octaethylporphyrin; MeIm, methylimidazole; MePip, methylpiperidine; TPivP, picket fence porphyrin; Me_2Im, dimethylimidazole.

[a] δ_{oop} Fe-out of plane towards nitrogen atom.

[b] B3LYP with Ahlrich's VDZ basis set.

be seen in the well-known *trans* effect, resulting in weak bonds to *trans* axial ligands [35]. In isomer I, the extra FeNO electron is transferred to the d_{z^2} orbital, where it reduces the σ bond order of the *trans* ligand bond. FeNO adducts are also unique in being oxidizable to $FeNO^+$, i.e. Fe(III)NO. The oxidized adducts are isoelectronic with FeCO.

DFT produces FeNO and FeO_2 geometries and vibrational frequencies that are in good agreement with experiment (Tables 1 and 2) [12]. The bond angles are accurately calculated, as are the metal–ligand distances. The single exception is the bond to the *trans* axial ligand in NO adducts. DFT calculates a near-normal Fe–N distance for a pyridine ligand, 2.07 Å, whereas the crystallographic distances for imidazole and piperidine ligands are 2.18 Å or greater. In addition, DFT predicts a significant lengthening of the Fe–NO bond upon pyridine binding, from 1.72 to 1.79 Å, whereas lengthening is not apparent in the crystallographic data. Thus, the data indicate that the σ competition for the d_{z^2} orbital between NO and the *trans* ligand is more heavily weighted than is predicted by DFT.

3.2. Backbonding

Despite their bonding and geometry differences, FeNO and FeO_2 show backbonding behavior quite similar to FeCO. When νFeX is plotted against νXO for a series of five-coordinate XO adducts of Fe(II) porphyrins with different substituents, straight lines with negative slopes are obtained for NO and O_2 as well as CO (Fig. 6). Of course, the XO frequencies are very different, but the range of frequencies for both νFeX and νXO are similar. Indeed, the slope of the backbonding correlation is the same for NO as for CO, and it is twice as large for O_2. (We

Table 2
Experimental and calculated vibrational frequencies (cm^{-1}) for XO adducts of Fe(II) porphyrins

Ligand	ν(X–O)		ν(Fe-XO)		δ(FeXO)		Reference
	Expt	DFT [a]	Expt	DFT	Expt	DFT	
Five-coordinate CO	1975 [b]	1985	531	581	–	(510, 510)	[36,37]
Six-coordinate CO	1970 [c]	1991	496	501	–	(572, 578) [d]	[38,39]
Five-coordinate NO	1669 [e]	1718	522	565	–	434	[12]
Six-coordinate NO	1591 [f]	1687	547	541	444	450	[40]
Five-coordinate O_2	1195 [g]	1159	508	702	349	347, 397 [h]	[42]
Six-coordinate O_2	1157 [i]	1176	575	623	–		[42]
	1207 [j]		488		279	268	[41]

OEP, octaethylporphyrin; Bz, benzene; ImH, imidazole; cyt, cytochrome; TPP, tetraphenylporphyrin; pip, piperidine; Pc, phthalocyanine.

[a] DFT, Fe(P) and Fe(P)py; all calculations reported are from Ref. [12].

[b] OEP in Bz.

[c] OEP(*N*-MeIm) in Bz.

[d] The two degenerate components of the bending mode (*E* in C_{4v} symmetry) are separated by the orientation of the *trans* ligand, py.

[e] OEP in Bz.

[f] Cyt P450.

[g] OEP, matrix.

[h] Normal coordinate analysis gives two modes with significant δ(FeXO) contribution.

[i] TPP(pip) in CH_2Cl_2 (ν(O–O)) and toluene (ν(Fe–O_2)).

[j] Pc, matrix.

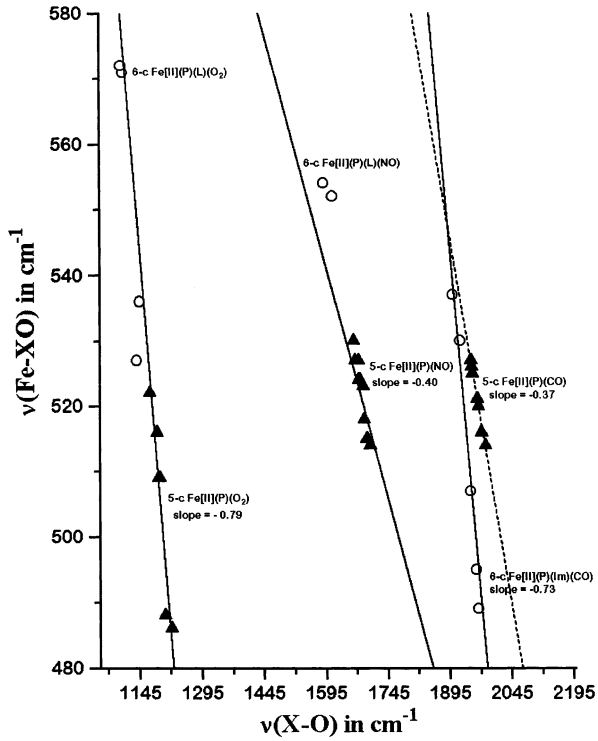

Fig. 6. Backbonding correlations between ν(Fe–XO) and ν(X–O) for five- (circles) and six-coordinate (triangles) XO adducts of Fe(II) porphyrins (from Ref. [12], where data references may be found).

note that the meaning of νFeX is not identical for the three XO molecules because for bent FeXO, there is kinematic mixing between the Fe–X stretching and Fe–X–O bending coordinates. The effect is to increase the separation of the two modes. However, this effect does not obscure the overall trends.)

The valence isomer model accommodates backbonding because even in the bent isomer II, there remains an empty π^* orbital perpendicular to the FeXO bending plane (Fig. 5). Since there are two d_π–π^* overlaps in isomer I and only one in isomer II, the extent of backbonding might have been expected to diminish from CO to NO to O_2. However, this trend is countered by stabilization of the π^* orbital along the same series, and this appears to be the more important effect.

3.3. Axial ligands

The effect of axial ligation on the νFeX/νXO frequencies is different for FeNO and FeO_2 than for FeCO. νXO is diminished in all three adducts, reflecting the increase in backbonding expected from the donor effect of the axial ligand. For FeNO and FeO_2, the diminished νXO is accompanied by an increase in νFeX, and the points fall on the backbonding correlations defined by the five-coordinate

adducts, but at higher positions on the lines (Fig. 6). This is the expected effect of changes in backbonding alone.

It is only for FeCO that axial ligation diminishes νFeX, at a given point on the backbonding correlation, and also increases the slope of the correlation (Figs. 1 and 6). As discussed above, these effects are due to σ competition between the axial ligand and CO lone pairs for the Fe d_{z^2} orbital. The absence of these effects for FeNO confirms the inference from the structural data (see above) that the axial ligand is unable to compete effectively with NO for σ bonding. This is apparently true for FeO_2 as well, although the absence of a five-coordinate crystal structure prevents evaluation of the effect of axial ligation on the Fe–O bond length. We infer that the NO and O_2 σ orbitals are better matched to the Fe d_{z^2} orbital than is the CO σ orbital, rendering the axial ligand less effective in the competition. Not surprisingly, DFT does not capture this effect, since, as seen in Table 2, it does not predict the axial ligand extension correctly in FeNO adducts. The DFT prediction is that νFeX decreases upon axial ligation for all three adducts [12], whereas the opposite is observed for FeNO and FeO_2 adducts.

4. Conclusions

The pattern of vibrational spectra for CO, NO and O_2 adducts of heme can be satisfactorily understood in terms of backbonding, as it is influenced by distal and proximal polarization effects, and changes in axial ligand donor character. DFT analysis helps to illuminate these trends, and can usefully model effects attributed to the surrounding protein. The situation is particularly favorable for heme–CO adducts for which there is a large database, and for which accurate theoretical results are obtained. Heme–NO and $-O_2$ adducts are less well understood, partly because the experimental data are more sparse, reflecting technical difficulties, and partly because they are more complex electronically, making theoretical analysis more problematic. These adducts are a challenge for future work.

References

[1] T.G. Spiro, P.M. Kozlowski, M.Z. Zgierski, J. Raman Spectrosc. 29 (1998) 896.
[2] E.A. Kerr, N.-T. Yu, in: T.G. Spiro (Ed.), Biological Applications of Raman Spectroscopy, vol. 3, Wiley, New York, 1998, pp. 39–96.
[3] G.B. Ray, X.-Y. Li, J.A. Ibers, J.L. Sessler, T.G. Spiro, J. Am. Chem. Soc. 116 (1994) 162.
[4] R. Evangelista-Kirkup, G. Smulevich, T.G. Spiro, Biochemistry 25 (1986) 4420.
[5] (a) D. Biram, C.J. Garratt, R.E. Hester, in: R.E. Hester, R.B. Girling (Eds.), Spectroscopy of Biological Molecules, Royal Society of Chemistry, Cambridge, UK, 1991, pp. 433–434;
(b) A.D. Cameron, S. Smerdon, A. Wilkinson, J. Habash, J.R. Helliwell, T. Li, J. Olson, J. Biochem. 32 (1993) 13061;
(c) T. Li, M.L. Quillin, G.N. Phillips Jr., J.S. Olson, Biochemistry 33 (1994) 1433.
[6] M. Unno, J.F. Christian, J.S. Olson, J.T. Sage, P.M. Champion, J. Am. Chem. Soc. 120 (1998) 2670.
[7] (a) B. Kushkuley, S.S. Stavrov, Biophys. J. 70 (1996) 1214;

(b) B. Kushkuley, S.S. Stavrov, Biophys. J. 72 (1997) 899.
[8] G.N. Phillips Jr., M. Teodoro, T. Li, B. Smith, M.M. Gilson, J.S. Olson, J. Phys. Chem. 103 (1999) 8817.
[9] X.-Y. Li, T.G. Spiro, J. Am. Chem. Soc. 110 (1988) 6024.
[10] K.M. Vogel, T.G. Spiro, D. Shelver, M.V. Thorsteinsson, G.P. Roberts, Biochemistry 38 (1999) 2679.
[11] K.M. Vogel, P.M. Kozlowski, M.Z. Zgierski, T.G. Spiro, Inorg. Chim. Acta 297 (2000) 11.
[12] K.M. Vogel, P.M. Kozlowski, M.Z. Zgierski, T.G. Spiro, J. Am. Chem. Soc. 121 (1999) 9915.
[13] P.M. Kozlowski, K.M. Vogel, M.Z. Zgierski, T.G. Spiro, J. Porph. Phthal. 5 (2001) 312–322.
[14] J. Kuriyan, S. Wilz, M. Karplus, G.A. Pestko, J. Mol. Biol. 192 (1986) 133.
[15] (a) X. Cheng, B.P. Schoenborn, Acta Crystallogr. Sect. B 46 (1990) 195;
(b) X. Cheng, B.P. Schoenborn, J. Mol. Biol. 220 (1991) 381;
(c) J.C. Norvell, A.C. Nunes, B.P. Schoenborn, Science 190 (1975) 568;
(d) J.C. Hanson, B.P. Schoenborn, J. Mol. Biol. 153 (1981) 117.
[16] (a) M.L. Quillin, R.M. Arduini, J.S. Olson, G.N. Phillips Jr., J. Mol. Biol. 234 (1993) 140;
(b) F. Young, G.N. Phillips Jr, J. Mol. Biol. 256 (1996) 762.
[17] G.S. Kachalova, A.N. Popov, H.D. Bartunik, Science 284 (1999) 473.
[18] J. Vojtechovsky, K. Chu, J. Berendzen, R.M. Sweet, I. Schlichting, Biophys. J. 77 (1999) 2153.
[19] M. Tsuboi, Indian J. Pure Appl. Phys. 26 (1988) 188.
[20] S. Hirota, T. Ogura, K. Shinawa-Itoh, S. Yoshikawa, M. Nagai, T. Kitagawa, J. Phys. Chem. 98 (1994) 6652.
[21] S. Hu, K.M. Vogel, T.G. Spiro, J. Am. Chem. Soc. 116 (1994) 11187.
[22] C. Rajani, J.R. Kincaid, J. Am. Chem. Soc. 120 (1998) 7278.
[23] A. Ghosh, D.F. Bocian, J. Phys. Chem. 100 (1996) 16.
[24] (a) T.G. Spiro, P.M. Kozlowski, J. Biol. Inorg. Chem. 2 (1997) 516;
(b) T.G. Spiro, P.M. Kozlowski, J. Am. Chem. Soc. 120 (1998) 4524.
[25] C. Rovira, M. Parrinello, Biophys. J. 78 (2000) 93.
[26] (a) D. Ivanov, J.T. Sage, M. Keim, J.R. Powell, S.A. Asher, P.M. Champion, J. Am. Chem. Soc. 116 (1994) 4139;
(b) J.T. Sage, Appl. Spectrosc. 51 (1997) 568;
(c) J.T. Sage, W. Jee, J. Mol. Biol. 274 (1997) 21.
[27] M. Lim, T.A. Jackson, P.A. Anfinrud, Science 269 (1995) 962.
[28] N. Godbout, R. Havelin, R. Salzman, P.G. Debrunner, E. Oldfield, J. Phys. Chem. A 102 (1999) 2342.
[29] (a) J.P. Collman, J.I. Brauman, T.R. Halbert, K.S. Suslick, Proc. Natl. Acad. Sci. USA 73 (1976) 3333;
(b) L. Stryer, Biochemistry (3rd ed.), 1988, Freeman, New York.
[30] B.A. Springer, S.G. Sligar, J.S. Olson, G.N. Phillips Jr., Chem. Rev. 94 (1994) 699.
[31] E. Sigfridson, U. Ryde, J. Biol. Inorg. Chem. 4 (1999) 99.
[32] T.G. Spiro, P.M. Kozlowski, Accts. Chem. Res. 34 (2001) 137.
[33] T.G. Spiro, Iron Porphyrins, Part Two, in: A.B.P. Lever, H.B. Gray (Eds.), Physical Bioinorganic Chemistry Series, Addison–Wesley, Reading, MA, 1982, pp. 89–159.
[34] R. Hoffman, M.M.-L. Chen, D.L. Thorn, Inorg. Chem. 16 (1977) 503.
[35] W.R. Scheidt, M.E. Frisse, J. Am. Chem. Soc. 97 (1975) 17.
[36] G.L. Woolerey, M.A. Walters, K.S. Suslick, L.S. Powers, T.G. Spiro, J. Am. Chem. Soc. 107 (1985) 2370.
[37] E.A. Kerr (Thesis), Georgia Institute of Technology, Atlanta, GA, 1984.
[38] Z. Yoshida, H. Sugimoto, H. Ogoshi, Adv. Chem. Ser. 191 (1980) 307.
[39] E.A. Kerr, H.C. Mackin, N.-T. Yu, Biochemistry 22 (1983) 4373.
[40] G. Deinum, J.R. Stone, G.T. Babcock, M.A. Marletta, Biochemistry 35 (1996) 1540.
[41] Y. Mizutani, S. Hashimoto, Y. Tatsuno, T. Kitagawa, J. Am. Chem. Soc. 112 (1990) 6809.
[42] L.M. Proniewicz, I.R. Paeng, K. Nakamoto, J. Am. Chem. Soc. 113 (1991) 3294.